Magnetic anisotropy under arbitrary excitation in finite element models

GREGOR BAVENDIEK, NORA LEUNING, FABIAN MÜLLER, BENEDIKT SCHAUERTE,
ANDREAS THUL, KAY HAMEYER

Institute of Electrical Machines (IEM), RWTH Aachen University
Schinkelstraße 4, 52056 Aachen, Germany
e-mail: gregor.bavendiek@iem.rwth-aachen.de

Abstract: Magnetic properties of silicon iron electrical steel are determined by using standardized measurement setups and distinct excitation parameters. Characteristic values for magnetic loss and magnetization are used to select the most appropriate material for its application. This approach is not sufficient, because of the complex material behavior inside electrical machines, which can result in possible discrepancies between estimated and actual machine behavior. The materials' anisotropy can be one of the problems why simulation and measurement are not in good accordance. With the help of a rotational single sheet tester, the magnetic material can be tested under application relevant field distribution. Thereby, additional effects of hysteresis and anisotropy can be characterized for detailed modelling and simulation.

Key words: magnetic anisotropy, material modeling, finite element method

1. Introduction

The magnetic conductivity of non-oriented soft magnetic electrical steel possesses an anisotropy. The response of magnetic polarization is dependent on the excitation direction of magnetic flux density. Next to hysteresis this effect is the reason for a phase shift between the magnetic field and magnetic flux density inside the material. Vector hysteresis models combine these effects, but unfortunately the state-of-the-art numerical test case [1] neglects the vector property of the magnetization/polarization angle, because it is based on single-sheet-tester (SST) measurements in different magnetization directions.

In this study the difference of conventional SST measurements, which include the amplitude response of the anisotropy, and rotational SST (RSST) measurements, which additionally include

the angular response of the anisotropy, is depicted for an exemplary, conventional M330-50A non-oriented electrical steel. Therefore, the full anisotropy information is modeled into the reluctivity tensor, which is derived by a multi-dimensional interpolation of ($\boldsymbol{BH}_{max}$) magnetization characteristics' measurements. Anisotropy can thus be considered decoupled from hysteresis, so that the latter is not part of this study. To concern rotational losses during electromagnetic machine simulation, which have become a prominent problem, a full vector hysteresis model as in [2] is recommended.

2. Measurement of vector magnetic anisotropy

2.1. Measurement topologies

The magnetic measurements in this paper are conducted on two different SST setups: A standard uniaxial SST and an RSST. For the 1-D characterization on the standard SST, rectangular samples cut in different angles between rolling direction (RD) and transverse direction (TD) are measured to determine the direction-dependent magnetic properties. Sample size is 120 mm × 120 mm and the field strength is determined indirectly by using the current-metric method. The 2-D uniaxial characterization is performed on an RSST. Here, four excitation coils placed on four magnetizing poles connected by a closing yoke generate the magnetic field [3]. The magnetic flux density inside the sample is measured by two orthogonal sensing coils in the center of a 60×60 mm sample, as depicted in Fig. 1. The nominal flux densities of the measurements are 0.1 T to 1.8 T in 0.1 T steps at a frequency of 50 Hz. The form factor is used as quality criterion for the comparability of the measurements. Uniaxial measurements with vector characteristics of $\boldsymbol{B}$ and $\boldsymbol{H}$ are performed on an RSST.
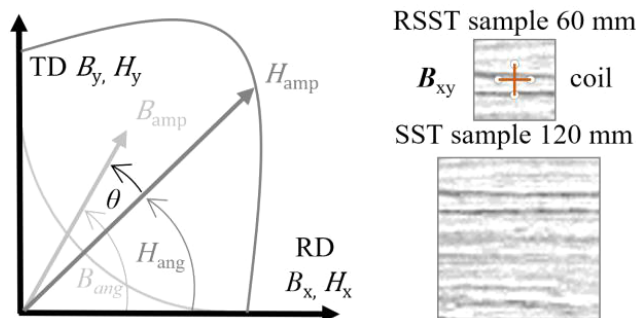

Fig. 1. Schematic illustration of the phase shift in vector $\boldsymbol{B}$ and $\boldsymbol{H}$ characteristics during SST and RSST measurements and geometry of samples
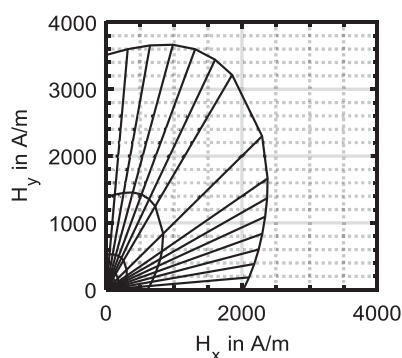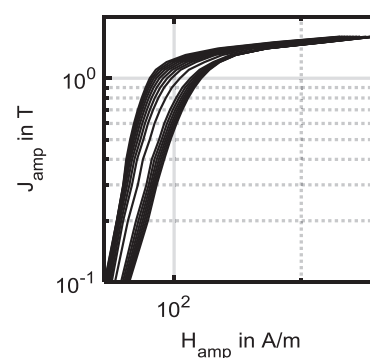
The difference of the two measurement setups is based on the information of the alignment or rather, the relative phase shift between the $\boldsymbol{H}$- and $\boldsymbol{B}$-vector (Fig. 1). The angle θ has to be identified, in order to properly analyze the orientation dependence of the material. $\boldsymbol{H}$- and $\boldsymbol{B}$-vector are considered to be collinear in standard SST setups, this is not the case due to the domain structure of the material. Due to the uniform alignment of the primary and secondary

coil, only the axial component of B is determined. In saturation, it is reasonable to assume collinearity, because of the domain rotation in the direction of the external field. The neglect of θ for polarizations below saturation is a substantial drawback of the measurement setup. At least for the amplitude of the measured quantities the measurements of the SST and RSST are qualitatively in good agreement. The amplitudes of the measured quantities are not supposed to be identical because of the different measurement approach. Also, the measurement accuracy makes it difficult to compare exact values of both devices. A direct correlation factor as it is set for standardized Epstein Frame and SST measurements is not yet determined for non-standardized RSST measurements.

2.2. Vector measurements on non-oriented electrical steel

The magnetic anisotropy of non-oriented electrical steels originates from the production process. This anisotropy is linked to various structural material parameters; such as grain size, crystallographic texture and global residual stress distribution [4]. Although not as pronounced as in grain-oriented electrical steels, an anisotropy in the entire sheet plane can still be denoted. Rolling, coiling and annealing in a continuous furnace are all axial production processes. This is the reason, why the steel strip data is distinguished by the RD and the TD direction. Slightly elongated, non-spherical grains and different residual mechanical stress in RD and TD as a result of the production, can contribute to the anisotropy. The main reason however, is the crystallographic texture, i.e., the orientation distribution of the single crystals in the polycrystalline material. The single-crystals already have a magnetic anisotropy with hard and easy magnetization directions. Deviations from the statistically ideal distribution of these crystals, i.e. the texture affect the anisotropy of the steel strip. The domain structure without an external field aligns along the easy magnetization axes. Thus, more energy is required for the domain wall movement and domain rotation if the magnetization vector is oriented farther from the easy axes compared with magnetization along a direction with many crystal orientations along easy axes.

The magnetic anisotropy changes with the amplitude and direction of magnetic flux density [4, 5]. In Fig. 2 alternating SST (a)–(d) and RSST (e)–(f) measurements in relative direction to RD = 0° are depicted next to each other. Booth measurement campaigns reveal a similar

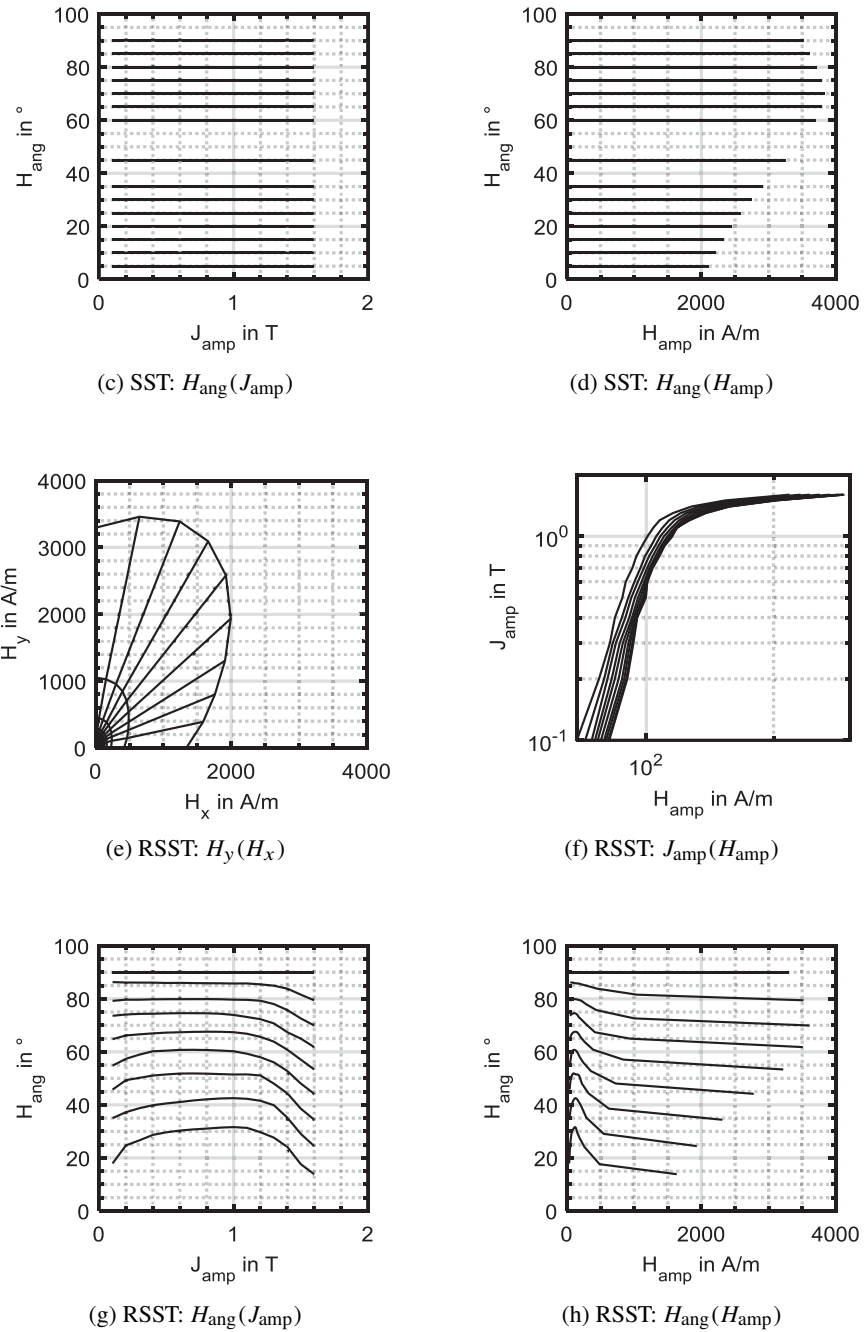(a) SST: $H_y(H_x)$ (b) SST: $J_{amp}(H_{amp})$

(c) SST: $H_{\mathrm{ang}}(J_{\mathrm{amp}})$

(d) SST: $H_{\mathrm{ang}}(H_{\mathrm{amp}})$

(e) RSST: $H_y(H_x)$

(f) RSST: $J_{\mathrm{amp}}(H_{\mathrm{amp}})$

(g) RSST: $H_{\mathrm{ang}}(J_{\mathrm{amp}})$

(h) RSST: $H_{\mathrm{ang}}(H_{\mathrm{amp}})$

Fig. 2. Response of magnetic field strength to controlled alternating magnetic flux density at 50 Hz with amplitudes ranging from $B_{\mathrm{amp}} = [0.1, \ldots, 1.6]$ T and angles from $B_{\mathrm{ang}} = [0, 10, 20, 30, (40, 50), 60, 70, 80, 90]°$

amplitude response, Fig. 2(a) and (e). From low up to medium magnetic flux densities the anisotropy in *x*- and *y*-direction often corresponds to an ellipse. Elliptical models [6] or related ones [7] can be used to model this dependence. At increasing magnetic flux density, a deviation from the ellipse can occur due to the dominance of texture. For the M330-50A with 2.4 wt.% FeSi measured in this paper, the hard magnetization axis is in the TD direction below 1 T and turns to 60° between 1 T and the saturation until the material becomes isotropic in high saturation. According to domain theory with increasing magnetization, the favorable oriented domains first grow and then rotate. Domains are generally oriented along the easy magnetization axes in the demagnetized state. At very high magnetic flux densities the material behaves increasingly isotropic, because the saturation magnetization is solely related to the chemical composition.

The most important difference between SST and RSST measurements can be seen in the angular dependencies of Fig. 2(c) vs. (g) and (d) vs. (h). With regular SST measurements, the magnetic field is induced vertically to the winding direction. Dependent on the sample cutting, this direction can be collinear to i.e. RD or TD or any other cutting direction. The induced voltage in the secondary winding is consequently also measured collinearly to the magnetic field. With this setup a tangential component of the magnetic flux density is thereby disregarded, and the angle of $\boldsymbol{H}$ is not measured and has to be assumed the same as for $\boldsymbol{B}$, Fig. 2(c) and (d). In contrast to that the RSST measures the quantities of $\boldsymbol{B}$ and $\boldsymbol{H}$ with two local perpendicular pickup coils each, which allows tracking of the angular response, Fig. 2(g) and (h). The amplitude and angle of the magnetic polarization can be deduced by the vector equation: $\boldsymbol{J} = \boldsymbol{B} - \mu_0\boldsymbol{H}$. For high values of the magnetic induction at saturation the angle of $\boldsymbol{B}$ and $\boldsymbol{H}$ become collinear again, but for lower values of magnetic induction, their phase shift θ is not zero and must not be neglected.

3. Finite element model with magnetic anisotropy

3.1. Representation of anisotropy in finite element method

The two-dimensional simulation of the TEAM problem 32 geometry is performed by solving a magneto-static vector potential formulation with the finite element method (FEM) by using the weak formulation of Ampere's law solved by a weighted residual approach with the weight functions $\boldsymbol{w}_j$ [8]. $\boldsymbol{A}$ is discretized by test functions $\boldsymbol{w}_i$, which take the same basis functions as $\boldsymbol{w}_j$. The curvature of Ω is given by $\partial\Omega$ and the source current density is only defined in the subspace Ω_s.

$$\int_{\Omega} \nu \nabla \times \boldsymbol{A} \cdot \boldsymbol{w}_j \, \mathrm{d}\Omega + \int_{\partial\Omega=\Gamma} \nu \nabla \times \boldsymbol{A} \times \boldsymbol{w}_j \, \mathrm{d}\Gamma = \int_{\Omega_s} \boldsymbol{J} \cdot \boldsymbol{w}_j \, \mathrm{d}\Omega_s \,. \tag{1}$$

The reluctivity ν is in general a strict positive semidefinite tensor and for isotropic materials it is reduced to a tensor without side entries and the same value on the main diagonal, which in fact means that it is equal to a scalar. The Newton method is applied, to take care of the nonlinear ferromagnetic materials. The Newton method calculates a correction $\Delta\boldsymbol{A}$ by linearizing the material behavior in the current working point. Depending on the nonlinear characteristic, the

method to determine the Jacobian is slightly different [8, 9]. Starting with a first linear step the linearization for the Newton Method is applied (2).

$$K \Delta A^k = J - \nabla \times H^{k-1}.$$ (2)

For isotropic regions the linearization for the Jacobian K is evaluated by (3).

$$\frac{\partial H}{\partial B} = \nu + 2 \frac{d\nu}{dB^2} B^2.$$ (3)

With (3) the entries of the Jacobian matrix in weak form can be written as in (4).

$$k_{ij} = \nu \nabla \times w_i \cdot \nabla \times w_j + 2 \frac{d\nu}{dB^2} (\nabla \times w_i \cdot \nabla \times A)(\nabla \times w_j \cdot \nabla \times A).$$ (4)

For anisotropic regions (5) is applied.

$$\nu_d = \frac{\partial H}{\partial B} = \begin{pmatrix} \dfrac{\partial H_x}{\partial B_x} & \dfrac{\partial H_x}{\partial B_y} \\ \dfrac{\partial H_y}{\partial B_x} & \dfrac{\partial H_y}{\partial B_y} \end{pmatrix}.$$ (5)

For anisotropic materials the Jacobian entries are determined as in (6).

$$k_{ij} = (\nabla \times w_i) \cdot \nu_d \cdot (\nabla \times w_j).$$ (6)

3.2. Direct modelling of anisotropy measurements within reluctivity tensor

The model holds information about the vector relationship between magnetic flux density excitation B and corresponding magnetic field H. The model provides accurate and smooth surfaces of magnetic field response on magnetic flux excitation, separated into Cartesian or Cylinder coordinates $H(B) = H_x(B)e_x + H_y(B)e_y = H_{amp}(B)e_r + H_{ang}(B)e_\varphi$. Directly from that the magnetic reluctivity tensor and its derivative are deduced as separate surfaces by using numerical gradients.

The first step is to clear the measured data from noise and regularize the surfaces in order to avoid convergence issues. This is done in Cylinder coordinates and then a transformation into Cartesian coordinates is performed by using *sine* and *cosine* functions of the measured angle. Here is the crucial part of SST measurements which assume the same angle $H_{ang} = B_{ang}$ and neglecting the angular response. The four-dimensional vector information $H(B)$ is covered by two surfaces, where the z-axis is the magnetic field in x- and y-direction H_x, H_y versus the magnetic flux in x- and y-direction. Fig. 3 shows all the mentioned surfaces for the data from [1], which has been extrapolated by saturated monotonous regression splines and extended by symmetry.

The entity surfaces of the reluctivity tensor are directly calculated by division of the magnetic field component by the magnetic flux density component, Fig. 4. The problems, which occur due to the division with zero in the reluctivity tensor, are corrected by a nearest neighbor interpolation. The entity surfaces of the differential reluctivity tensor are obtained by the numerical gradient of the reluctivity tensor entities, Fig. 5.
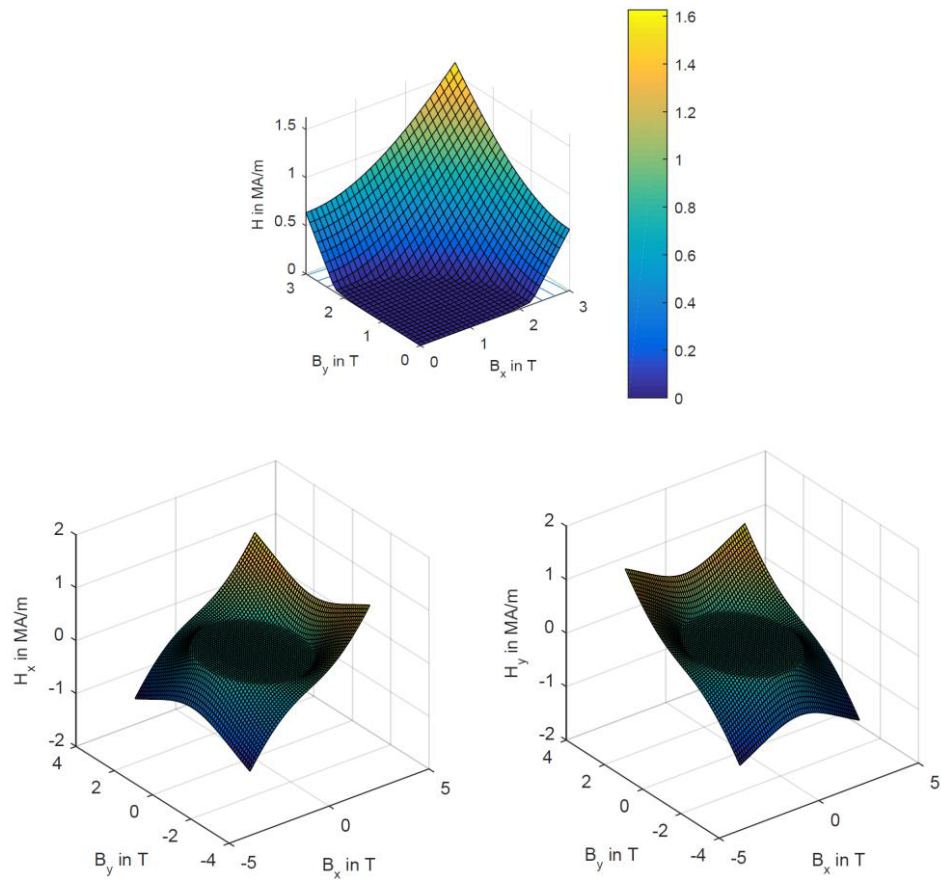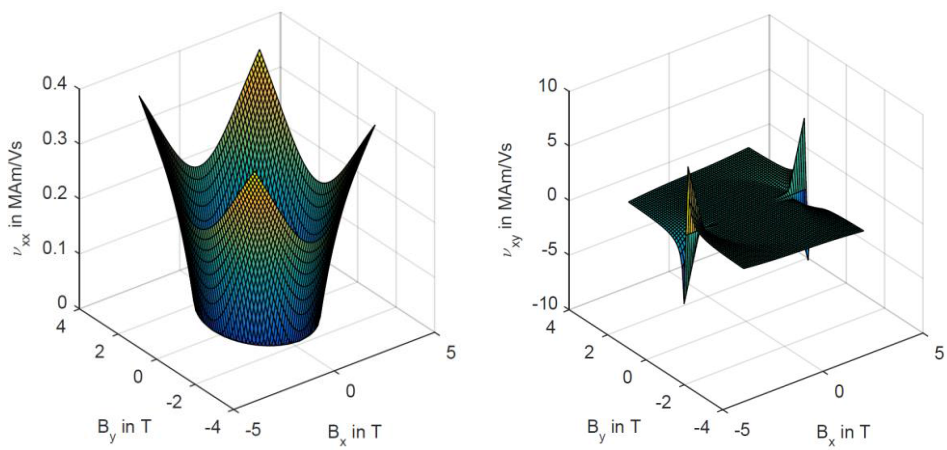
Fig. 3. Model applied to amplitude response data of TEAM problem 32 [1]
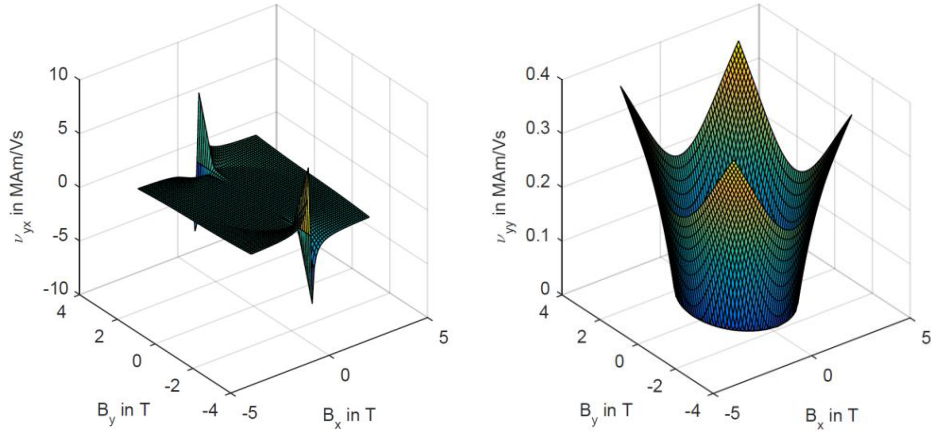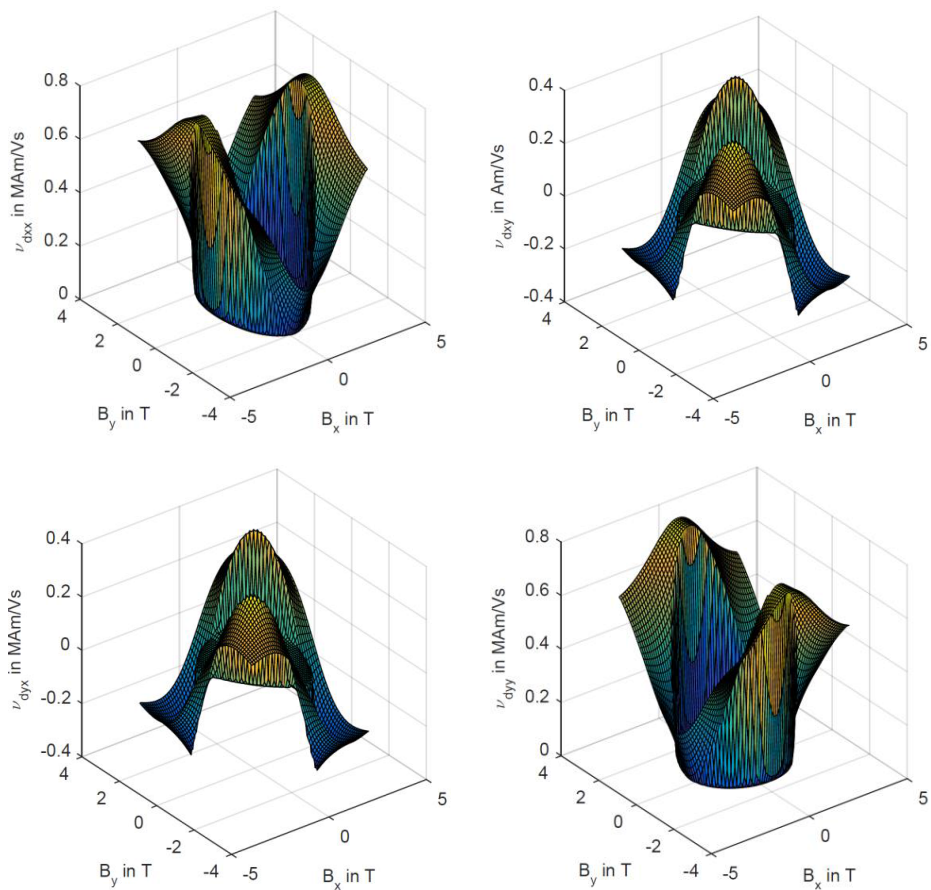
Fig. 4. Derived entities of reluctivity tensor

Fig. 5. Derived entities of differential reluctivity tensor

4. Simulation of numerical test case considering full vector anisotropy

4.1. Application of the model to pure SST measurements and rotational magnetization

In [1] four exemplary test cases containing alternating and rotating magnetic flux are described. In this paper, case 3, a sinusoidal current excitation with 90° phase shift between the limbs is calculated. This causes a rotational flux density locus in the transformers middle T-joint. The proposed model is applied to the original SST data of [1] and the simulation results are shown in Fig. 6. The loci of the magnetic field and magnetic flux density are evaluated in each element at every time step and plotted for the upper T-joint region in (a). The shape of the loci depends on the position and size of the discretized elements, therefore, a comparison of the simulation to the measurement of the B pick-up coils at point P2 reveals a good approximation.

(a) H and B loci in T-joint
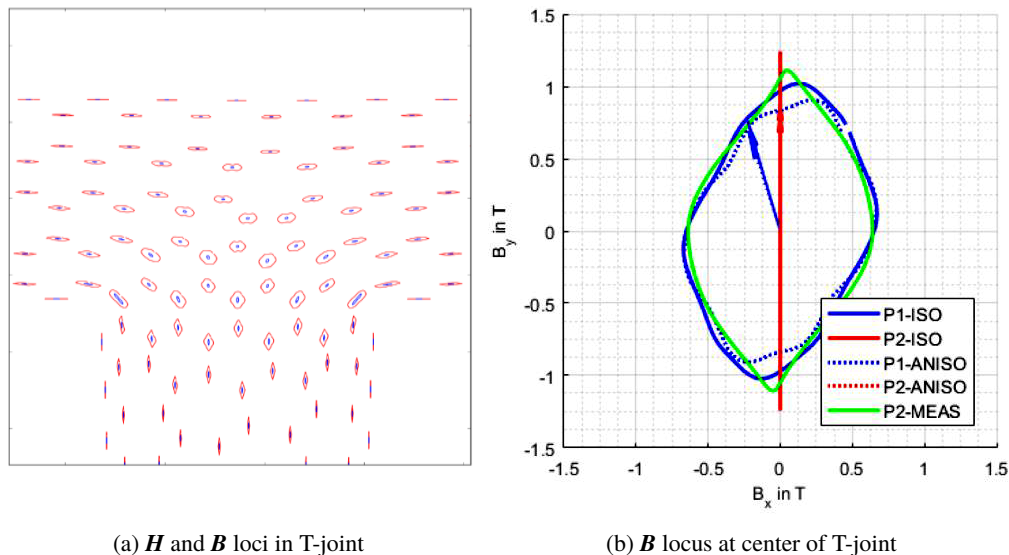
(b) B locus at center of T-joint

Fig. 6. Simulation of anisotropic material model for rotational locus from [1]

4.2. Comparison of the model for the performed SST and RSST measurements

In Fig. 7 the surfaces which contain the vector correlation, separated in amplitude and angle, between the magnetic field strength and magnetic flux density are shown in top view comparing SST (left) and RSST (right). The surfaces are optically slightly different due to the variation in scale, but particularly for small polarizations significant deviations occur locally both, in the amplitude and in the angle. In strong saturation ($J > 2$ T) the amplitude and angle continue to approach isotropic behavior in booth measuring devices. The expected distortion is best seen in the angular behavior of $H_{\mathrm{ang}}(B)$, which deviates strongly especially for small amplitudes of B.

In contrast to [1] which only provides SST measurements, in this paper the above introduced SST and RSST measurements of a silicon steel with 2.4% silicon are compared. To underline the influence of the phase lag between B and H, the comparative simulation is done with same amplitude characteristic (mean of Fig. 7(a), (c), but on the one hand with the constant angle characteristic of the SST (4(b)) and on the other hand with the non-linear angle characteristic of the RSST (4(d)).
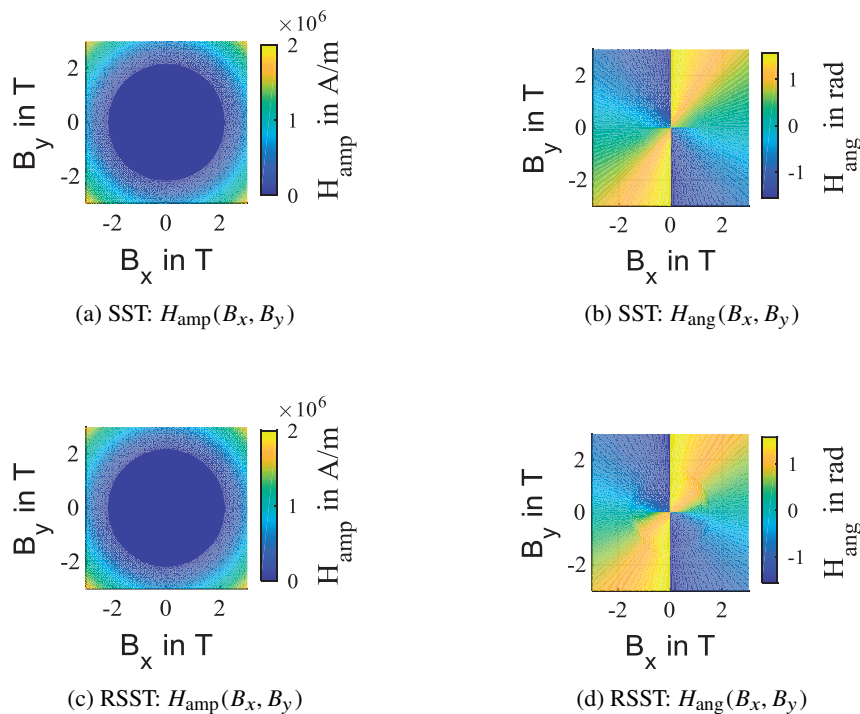

(a) SST: $H_{\mathrm{amp}}(B_x, B_y)$

(b) SST: $H_{\mathrm{ang}}(B_x, B_y)$

(c) RSST: $H_{\mathrm{amp}}(B_x, B_y)$

(d) RSST: $H_{\mathrm{ang}}(B_x, B_y)$

Fig. 7. $H(B)$ surfaces for SST (left) and RSST (right)

In Fig. 8 the loci of magnetic field and magnetic flux density are depicted in (a) and (b) for a full simulated period at the T-joint. The simulation of RSST with angle θ is marked by dots. The simulation of SST without angle θ has no marker. The phase shift θ is visualized by arrows for one simulation step at a quarter of the period length. The corresponding magnetization curves in x- (smaller amplitude) and y- (larger amplitude) direction are given in (c). The local vector plots are shown in (d) for SST and (e) for RSST. The magnetic field vectors are blue and the magnetic flux density vectors are red. The difference of the magnetic flux density between the simulation with and without θ is represented in (f), the color of each element gives the absolute difference in amplitude and the vectors (red) the direction. Since the absolute value of the flux density is around 1 T, the relative deviation in some elements is about 10%. Even if the total magnetization changes only slightly, the local impact is not negligible.
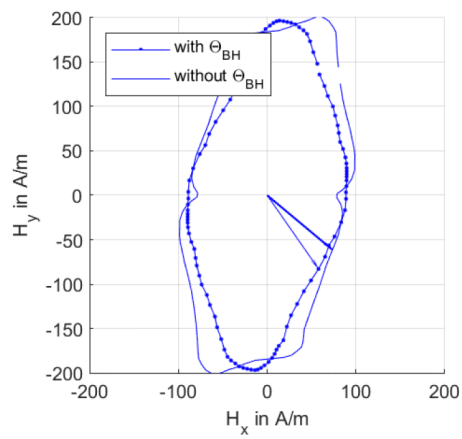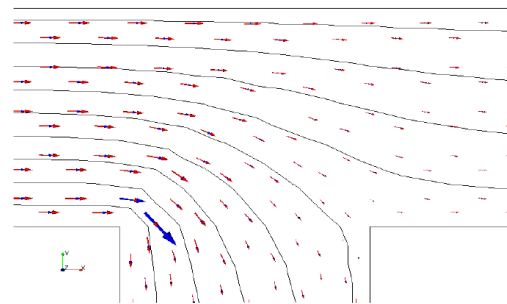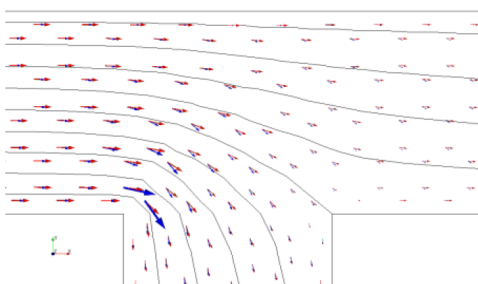
(a) Mag. field loci
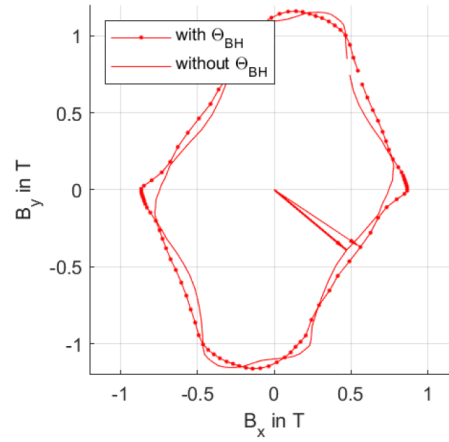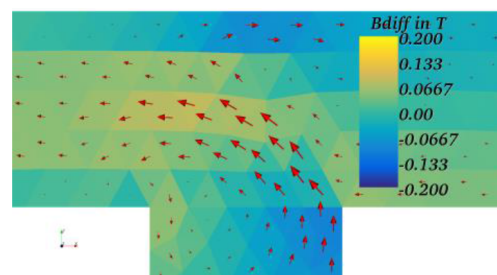

(b) Mag. flux density loci
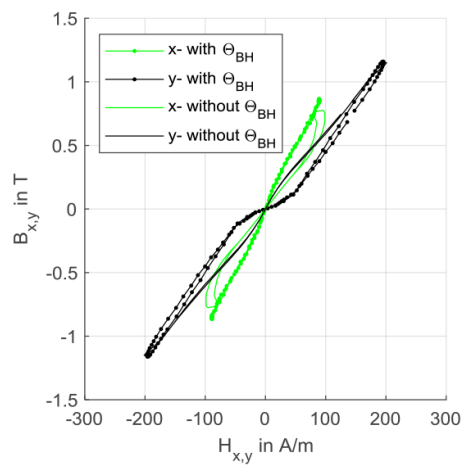
(c) Magnetization in T-joint

(d) SST simulation

(e) RSST simulation

(f) Difference in *B* due to θ

Fig. 8. Difference of SST and RSST model on local *B-H* curves in T-joint

5. Conclusions

In this paper the difference of SST and RSST measurements concerning the phase shift θ between $\boldsymbol{B}$ and $\boldsymbol{H}$ is discussed on the TEAM problem 32 geometry. The magnetic anisotropy is represented inside the reluctivity tensor by interpolated surfaces reconstructed out of amplitude and angle measurements. The full reluctivity tensor is derived by a multidimensional interpolation of the $\boldsymbol{BH}_{\max}$ magnetization characteristic. The vector mapping of $\boldsymbol{H}(\boldsymbol{B})$ is performed by splitting up into the two surfaces $\boldsymbol{H}(\boldsymbol{B}) = H_x(\boldsymbol{B})\mathbf{e}_x + H_y(\boldsymbol{B})\mathbf{e}_y = H_{\mathrm{amp}}(\boldsymbol{B})\mathbf{e}_r + H_{\mathrm{ang}}(\boldsymbol{B})\mathbf{e}_\varphi$. First, the measurements are conditioned for the nonlinear interpolation scheme by extrapolated regression splines over amplitude and angle. Second, the surfaces are a linear interpolation of scattered points in Cylinder coordinates and stored as a dense lookup table in Cartesian coordinates which are bilinear interpolated during solving. Although the surfaces here make a model unnecessary, the raw data can, of course, also be obtained from a model. Directly from the $H_x(\boldsymbol{B})$ and $H_y(\boldsymbol{B})$ surfaces the reluctivity tensor, for linear step, and differential reluctivity tensor, for nonlinear step, are derived by the quotient and the gradient. If hysteresis shall be considered, the proposed approach can be combined with a vector stop hysteresis model.

References

[1] Bottaus O., Ragusa C., Rege L., Chiamp M., *A test-case for validation of magnetic field analysis with vector hysteresis*, IEEE Transactions on Magnetics, vol. 38, no. 2, pp. 893–896 (2002).

[2] Alatawneh N., Pillay P., *Modeling of the interleaved hysteresis loop in the measurements of rotational core losses*, Journal of Magnetism and Magnetic Materials, vol. 397, pp. 157–163 (2016).

[3] Thul A., Steentjes S., Schauerte B., Klimczyk P., Denke P., Hameyer K., *Rotating magnetizations in electrical machines: Measurements and modeling*, AIP Advances, vol. 8, no. 5, p. 56815 (2018).

[4] Barros J., Schneider J., Verbeken K., Houbaert Y., *On the correlation between microstructure and magnetic losses in electrical steel*, Journal of Magnetism and Magnetic Materials, vol. 320, no. 20, pp. 2490–2493 (2008).

[5] Landgraf F.J.G., Yonamine T., Emura M., Cunha M.A., *Modelling the angular dependence of magnetic properties of a fully processed non-oriented electrical steel*, JMMM, vol. 254–255, pp. 328–330 (2003).

[6] Dedulle J.M., Meunier G., Foggia A., Sabonnadiere J.C., Shen D., *Magnetic fields in nonlinear anisotropic grain-oriented iron-sheet*, IEEE Transactions on Magnetics, vol. 26, no. 2 (1990).

[7] Lin D., Zhou P., Badics Z., Fu W.N., Chen Q.M., Cendes Z.J., *A new nonlinear anisotropic model for soft magnetic materials*, IEEE Transactions on Magnetics, vol. 42, no. 4, pp. 963–966 (2006).

[8] Krüttgen C., Steentjes S., Glehn G., Hameyer K., *Parametric Homogenized Model for Inclusion of Eddy Currents and Hysteresis in 2-D Finite-Element Simulation of Electrical Machines*, IEEE Transactions on Magnetics, vol. 53, no. 6, pp. 1–4 (2017).

[9] Gyselinck J., Dular P., Sadowski N., Leite J., Bastos J.P.A., *Incorporation of a Jiles-Atherton vector hysteresis model in 2D FE magnetic field computations*, COMPEL, vol. 23, no. 3, pp. 685–693 (2004).